MODELING OF TURBULENT MELT CONVECTION DURING CZOCHRALSKI BULK CRYSTAL GROWTH

Vladimir V. Kalaev and Alexander I. Zhmakin
Numerical Simulation Department, Ioffe Physical Technical Institute
26 Polytekhnicheskaya, 194021, St.Petersburg, Russia
kalaev@softimpact.fi.ru

Eugene M. Smirnov
Aerodynamics Department, State Technical University
195251, St.Petersburg, Russia
aerofmf@citadel.stu.neva.ru

ABSTRACT

We present the results of numerical simulation of 3D unsteady turbulent melt convection during Czochralski (CZ) silicon crystal growth. A model combining the Large Eddy Simulation (LES) and Reynolds-averaged approaches has been developed to predict the contribution of unresolved turbulent motion. The model is examined for different growth conditions in an industrial CZ configuration. Data illustrating instantaneous and time-averaged behavior of the melt are presented and compared to experimental observations. Thermal fluctuations in the melt are analyzed with respect to spectral characteristics and compared to the temperature measurements performed by thermocouples and an optical sensor.

INTRODUCTION

The majority (about 98 %) of monocrystalline silicon wafers used in electronics is produced by the Czochralski method with the crystal pulled vertically from the turbulent melt. The intensity of turbulent convection in the melt determines directly the heat transfer through the melt and the crystallization rate at the melt-crystal interface. Natural convection due to the temperature gradients in the gravity field is combined with the effects induced by crystal rotation and by rotation of the crucible containing the melt (see Fig.1 for a CZ system schematic view). The melt convection on the free surface is affected by Marangoni tension and by shear stress induced by flow of the inert gas supplied along the melt surface for avoiding impurity deposition on the crystal surface. Turbulent coherent structures near the melt free surface control the impurity exchange between the melt and the inert gas. On the other hand, up-to-date CZ systems to grow crystals of 300mm in diameter are magnetic-field-applied for damping intensive natural convection. So, the melt turbulent flow during industrial crystal growth is affected by a wide variety of physical phenomena that should be investigated and made controllable.

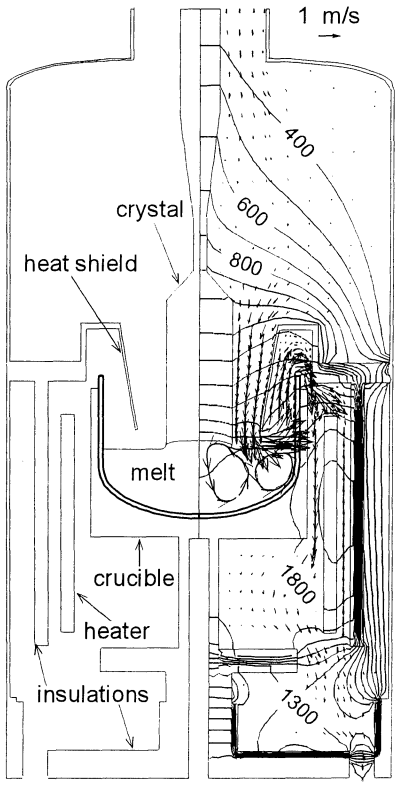

Figure 1. Schematic configuration of a CZ system for growth of silicon crystals of 100 mm in diameter (left). Temperature distribution (given in Kelvin) and argon velocity map in the system (right).

During the last two decades, there has been much interest in the calculation of turbulent melt convection because the conventional experimental approach becomes extremely expensive to be used in the adjustment of crystal growth for newly designed CZ systems. Most researchers deal with the axisymmetrical approximation describing turbulent mixing in terms of the Reynolds-averaged Navier-Stokes (RANS) approach involving a turbulence model to define the effective viscosity. Assaker et al.

(1997) presented time-depended calculations of silicon crystal growth by the CZ method using a simplified algebraic turbulence model for melt convection. Egorov et al. (1998) applied a low-Re turbulence model of the k-ε type to define the turbulent viscosity; however, global heat transfer and melt convection were not calculated self-consistently. A special study has been performed by Lipchin and Brown (1999) to understand which turbulence model is the best for melt convection simulation. They examined a simplified crucible geometry and uniform thermal boundary conditions with the conclusion that the low-Re model of Jones-Launder is preferable with respect to the prediction of bulk flow and impurity transport through the melt. This model was used (Lipchin and Brown, 2000) to calculate the global heat and mass transport in a CZ system; however, the inert gas flow through the system was ignored. Kalaev et al. (2000) have presented the calculations of global heat and mass transfer in a CZ system for growth of 100 mm Si crystals. They accounted for turbulent melt convection, inert gas flow, radiative heat exchange, and conduction in the solid parts, obtaining a self-consistent numerical solution. The low Reynolds number turbulence model of Chien (1982) was used in the calculations.

Despite the significant progress achieved in the numerical analysis in recent years, a comparison of calculations and measurements (temperature data, the impurity concentration in the crystal, the melt-crystal interface geometry) shows that the quasi-steady axisymmetric approximation often fails to provide a technologically desired predictability (see, for example, Müller et al., 1999 and Mühe et al., 1999). Nowadays, the commonly accepted point of view is that unsteady three-dimensional melt fluctuations during the crystallization process have specific features that can not be described well by conventional turbulence models operating with the isotropic effective turbulent viscosity. Therefore, the interest in 3D unsteady numerical simulation of turbulent melt convection rapidly grows with increasing computer resources. The first attempts to predict 3D unsteady melt convection were performed using the Direct Numerical Simulation (DNS) technique which requires no turbulence models (see Kishida and Okazawa, 1999, Basu et al., 2000, and references within). However, attempts aimed at resolving most turbulent eddies in an industrial melt necessitate the use of extremely extensive computational grids (10^6 - 10^9 cells) because the Grashof number is in the range of 10^9 to 10^{10}.

The employment of LES is an alternative to extensive DNS calculations. A Sub-Grid Scale (SGS) turbulence model is required to calculate effective viscosity describing turbulent eddies unresolvable by LES. The computational grid should be sufficient to resolve just energetic large-scale turbulent vortices largely governing heat and mass transport. However, the traditional LES approach may fail to calculate heat and mass transport near solid walls due to the absence of statistical balance of turbulence dissipation. To provide a more accurate prediction for the melt core and for the near-wall layers, we present a combined LES/RANS model. The model has been applied for melt flow calculations in an industrial CZ system and verified by available experimental data.

MATHEMATICAL MODEL

To describe the buoyancy-driven motion, the Boussinesq approximation of the Navier-Stokes equations is used in combination with the energy equation

$$\nabla \cdot \vec{u} = 0 \tag{1}$$

$$\rho \frac{d\vec{u}}{dt} = -\nabla p + \nabla \cdot \hat{\tau} + \rho \beta (T_0 - T)\vec{g} \tag{2}$$

$$\hat{\tau} = 2(\mu + \mu_t)\dot{S}$$

$$\rho \frac{dT}{dt} = \nabla \cdot \left(\left(\frac{\mu}{\mathrm{Pr}} + \frac{\mu_t}{\mathrm{Pr}_t}\right)\nabla T\right) \tag{3}$$

In the equations, u is the melt velocity, ρ is the density, T is the temperature, p is the reduced pressure, β is the thermal expansion coefficient, S is the strain-rate tensor, μ is the Si melt dynamic viscosity, μ_t is the turbulent effective viscosity, g is the gravity vector, T_0 is the melt reference temperature, Pr is the Prandtl number of silicon, and Pr_t is the turbulent Prandtl number taken to be 0.4.

The crucible and crystal rotation effects on melt convection are accounted for by imposing non-zero angular velocities on respective boundaries. The normal velocity component over the melt free surface is set to be zero and the longitudinal velocity components should satisfy the following condition:

$$\mu \frac{\partial \vec{u}_\tau}{\partial n} = \mu_g \frac{\partial \vec{u}_{\tau_g}}{\partial n} + \frac{\partial \sigma}{\partial T} grad_\tau(T) \tag{4}$$

Here the subscript g is for the gas variables, n and τ are the normal and longitudinal directions, and σ is the surface tension coefficient of the Si melt. The first term in the right part of expression (4) accounts for the gas shear stress while the second term defines the Marangoni effect. The melt physical properties borrowed from the references mentioned above are listed in Table 1.

Melting temperature, K	1685
Density, kg/m^3 (at $T_{melting}$)	2570
Dynamic viscosity, Pa s	$8 \cdot 10^{-4}$
Thermal conductivity, W/Km	66.5
Specific heat, J/Kkg	915
Thermal expansion coefficient, 1/K	$1.44 \cdot 10^{-4}$
Temperature dependence of density, kg/m^3	3194-0.3701·T
$d\sigma/dT$, N/Km	$-1.5 \cdot 10^{-4}$
Emissivity	0.3

Table 1. Si melt physical properties.

The thermal boundary conditions are formulated as follows. The melt-crystal interface temperature is fixed at the melting temperature level. Using the data obtained by an axisymmetric model of global heat and mass transfer, the incoming radiative heat flux along the free surface is preset and the outcoming radiative heat flux is calculated from the surface temperature and the melt emissivity. An external heat transfer boundary condition is used to simulate the melt heating by the quartz crucible.

To calculate the effective melt viscosity in the melt core, we employ an algebraic SGS model of the Smagorinski type

$$\nu_t = (C\Delta)^2 \sqrt{2\bar{S}^2 + \beta_t \vec{g} \cdot grad(T)/\mathrm{Pr}_t} \qquad (5)$$

The constant C is chosen to be 0.13, the length scale Δ is equal to the double medial diagonal of a hexahedral computational cell.

To describe turbulent mixing in the vicinity of solid boundaries, we have applied the low-Re k-ε turbulence model of Chien (1982) with some modifications

$$\rho \frac{dk}{dt} = \nabla \cdot ((\mu + \frac{\mu_t}{\sigma_k}) \nabla k) + (P - \varepsilon - D) \qquad (6)$$

$$\rho \frac{d\varepsilon}{dt} = \nabla \cdot ((\mu + \frac{\mu_t}{\sigma_\varepsilon}) \nabla \varepsilon) + C_{\varepsilon_1} f_1 \frac{P\varepsilon}{k} - C_{\varepsilon_2} f_2 \frac{\rho \varepsilon^2}{k} + E \qquad (7)$$

$$P = 2\mu_t \dot{S} \cdot \nabla \vec{u} + \beta \vec{g} \cdot \frac{\mu_t}{\mathrm{Pr}_t} \nabla T \qquad (8)$$

$$\mu_t = C_\mu f_\mu \rho k^2 / \varepsilon \qquad (9)$$

$$C_\mu = 0.09 \quad C_{\varepsilon_1} = 1.35 \quad C_{\varepsilon_2} = 1.8 \quad \sigma_k = 1.0 \quad \sigma_\varepsilon = 1.3 \qquad (10)$$

$$f_\mu = 1 - \exp(-0.0115 y^+) \qquad f_1 = 1.0 \qquad (11)$$

$$f_2 = 1 - 0.22 \exp\left[-(\frac{\mathrm{Re}_t}{6})^2 \right] \qquad (12)$$

$$D = \frac{2\mu k}{y^2} \qquad E = -2\mu(\frac{\varepsilon}{y^2}) \exp(-0.5 y^+) \qquad (13)$$

Here, y^+ is the conventional dimensionless coordinate and y is the distance to the wall. The turbulence production owing to buoyancy is taken into account by equation (8). The zero-value conditions are imposed on k and ε at solid boundaries. For the melt free surface, the zero-flux boundary condition is chosen as a suitable variant.

The present hybridization of the LES and RANS approaches consists in choosing a minimum effective viscosity given by the SGS model and the "complete" turbulence viscosity at any point. Practically, the SGS model is activated in the melt because of a high effective viscosity rate produced by the k-ε model. On the other hand, the low-Re k-ε model generates a reasonable effective viscosity near solid walls with a proper lowering at the viscosity down to the molecular level at the wall.

The external boundary conditions for the 3D calculations have been provided by the model of global heat and mass transport based on the quasi-steady axisymmetric approach (Egorov et al., 1998, Kalaev et al., 2000). The finite volume method on block-structured grids has been applied to the 3D calculations, using a customized version of the CFD-ACE code (CFD-ACE is the product of CFD Research Corporation, Huntsville, AL, USA; http://www.cfdrc.com).

RESULTS

Global heat and mass transport in the EKZ-1300 CZ system considered previously by Dornberger et al. (1997) has been numerically simulated to provide thermal boundary conditions and gas shear stress distribution along the melt free surface. The temperature distribution and the inert gas velocity map are presented in Figure 1 (right) for the following operating conditions. The crucible rotation rate is 5 rpm, the crystal rotation in the counter direction is 20 rpm, the inert gas pressure and flow rate are 30 mbar and 675 slh, respectively, the crystallization rate is 1.9 mm/min, the crystal diameter is 100 mm. It should be noted that there are strong gradients of gas velocity near the melt free surface, affecting melt convection. The gas shear stress has been found to be stronger than the Marangoni tension along the free surface.

The computational grid (of about 65 000 cells) used for the 3D unsteady analysis is illustrated in Figure 2. This grid is found to be sufficient to resolve large turbulent structures in the melt.

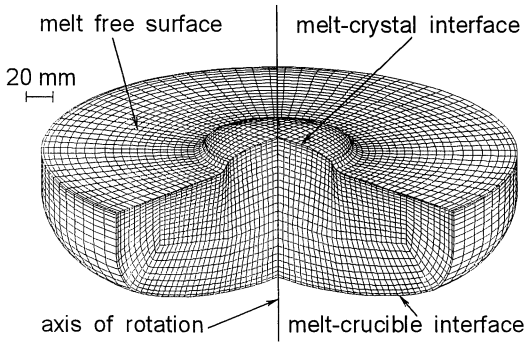

Figure 2. 3D block-structured computational grid used for LES of the melt.

Using the hybrid LES/RANS turbulence model, two computations were made by a personal computer. The crucible rotation rates were adopted to be 2 and 5 rpm, with the other conditions being fixed at the values given above. To obtain the boundary conditions, both regimes were calculated in terms of the model of global heat and mass transfer. The time step was chosen to be 0.5 s. A transient time period of about 800 seconds was calculated and a time interval of about 1000 seconds was used for obtaining time-averaged distributions and spectral characteristics. All instantaneous distributions to be presented below are for the last time step of a respective run.

Figure 3 and 4 illustrate the temperature, velocity, and effective viscosity distributions in a vertical cross-section for the crucible rotation rates of 2 and 5 rpm, respectively.

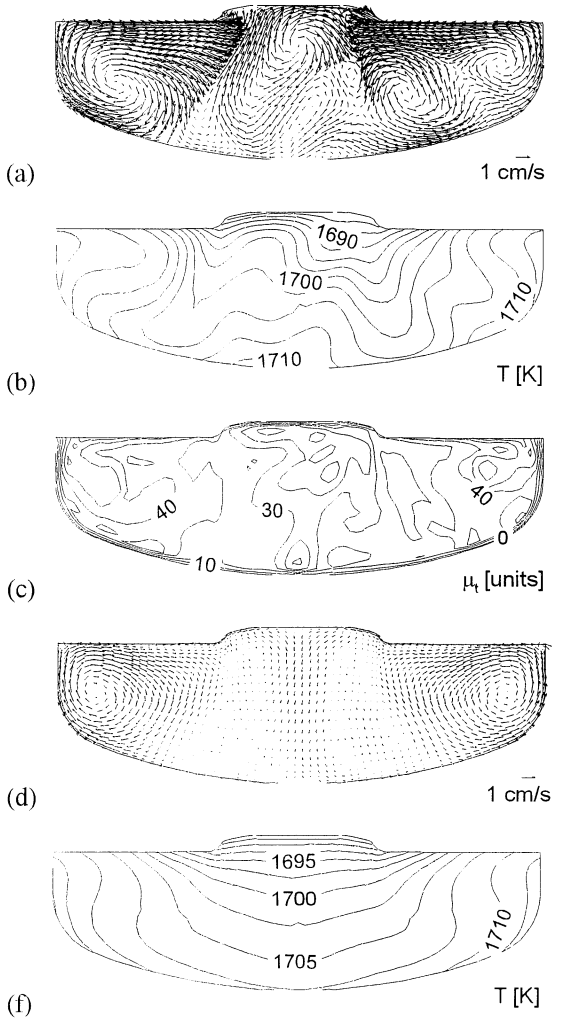

Figure 3. Instantaneous distributions of the velocity (a), temperature (b), and dimensionless effective viscosity (c); time-averaged distributions of the velocity (d) and temperature (f). The crucible rotation is 2 rpm.

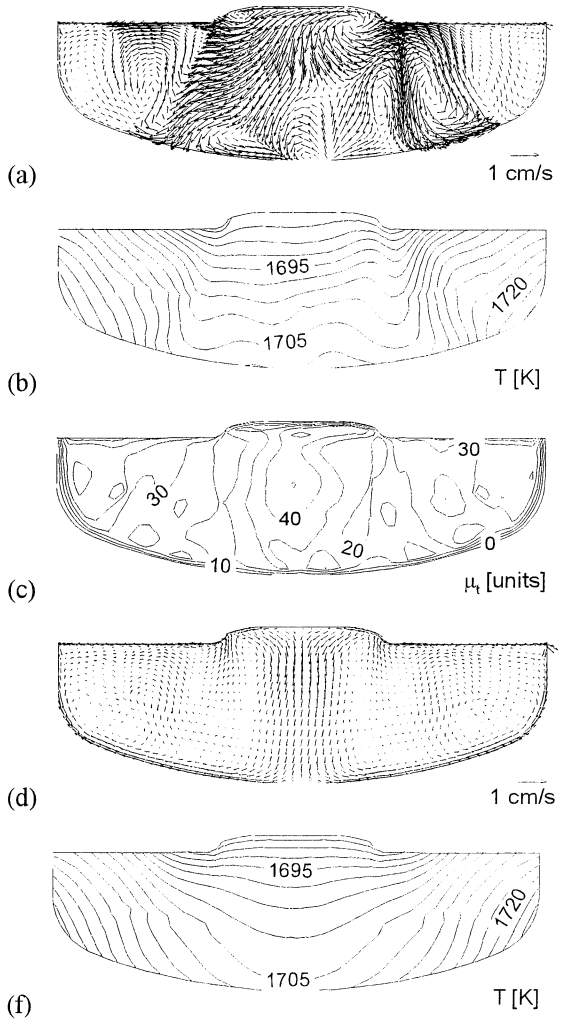

Figure 4. Instantaneous distributions of the velocity (a), temperature (b), and dimensionless effective viscosity (c); time-averaged distributions of the velocity (d) and temperature (f). The crucible rotation is 5 rpm.

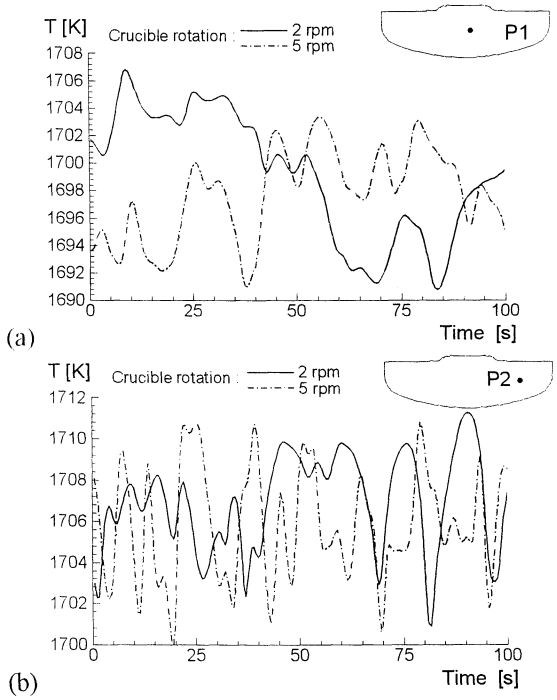

Figure 5. Calculated temperature fluctuations at two monitoring points for various crucible rotation rates.

When comparing the instantaneous velocity distributions, it should be emphasized that an increase in the crucible rotation rate results in a significant suppression of natural melt convection on the melt periphery. Secondly, turbulent convection for the slower crucible rotation is well developed in the whole melt domain and its intensity is twice as high as that for the crucible rotation of 5 rpm. This is responsible for a pronounced convection effect on the instantaneous temperature distribution for the slower crucible rotation. The effective turbulent viscosity distributions look very similar in both regimes. The effective viscosity rises from zero at the solid walls to an average of 20 - 30 units of the molecular viscosity. The time-averaged temperature and velocity distributions also point to an intensive natural convection on the melt periphery for the slower crucible rotation. Nevertheless, the time-averaged velocity distribution for 5 rpm shows a very slow melt motion compared to the instantaneous motion for this regime and to the averaged motion for the slower crucible rotation. This results in a greater temperature difference in the melt for 5 rpm. The predicted temperature difference is equal to 40 K for this regime and correlates well (within 5 K) with the temperature measurements by thermocouples, presented by Seidl et al. (1998). Also, the experimentally observed tendency of fluctuation suppression on the melt periphery is reproduced well by our calculations.

To provide a better insight into the behavior of temperature fluctuations affecting the crystal growth and, consequently, the monocrystalline substrate

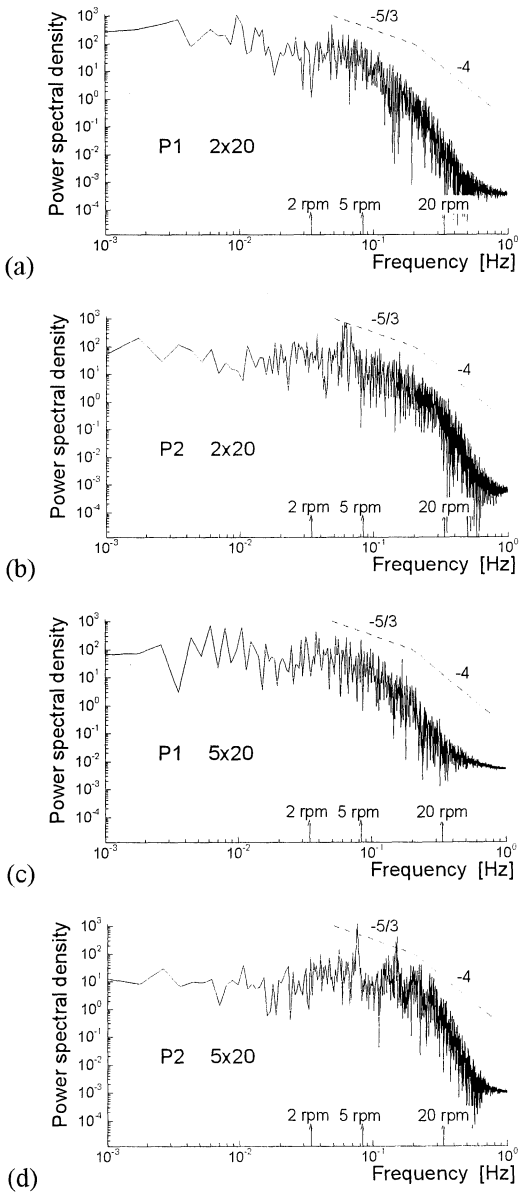

Figure 6. Power spectral density distributions of temperature fluctuations at monitoring points. The crucible rotation rate is 2 rpm, point P1 (a) and point P2 (b). The crucible rotation rate is 5 rpm, point P1 (c) and point P2 (d).

yield, we have analyzed the time evolution of temperature at two points inside the melt core. The positions of these stationary monitoring points and the temperature fluctuations in both calculated regimes are presented in Figure 5 for a sample time period of 100 seconds. One point P1 is placed in the under-crystal region and the other point P2 is positioned near the melt periphery. It is evident that the temperature evolution is chaotic in time for both regimes. However, there is a significant difference between the melt regions under analysis. The characteristic fluctuation frequency is higher in the vicinity of P2 for both regimes; however, the higher crucible rotation rate suppresses the long-period melt

fluctuations at both points, which is in good agreement with experimental observations (Gräbner et al., 2000).

The calculation of the power spectra of the temperature fluctuations provides a better understanding of turbulent convection mechanisms. Figure 6 illustrates the Power Spectral Density (PSD) distributions calculated from the fluctuations saved during the time period of 1000 seconds. Any dominating frequency peaks correlating with the crucible or crystal rotation rates are not observed in our calculations, which is similar to the measurement by thermocouples (Seidl et al., 1998) and by an optical sensor (Gräbner et al., 2000). Also, it should be noted that fully developed turbulence conditions have not been reached in the melt flows. However, the PSD distribution at P2 for the lower crucible rotation is closely proportional to $f^{-5/3}$. The increase in the crucible rotation leads to significant changes in PSD on the melt periphery. The calculations reveal a suppression of high frequency oscillations in the under-crystal region with increasing crucible rotation; besides, the turbulence spectra are found to be proportional to f^{-4}, which indicates the development of weak turbulence.

CONCLUSIONS

We have developed an efficient model based on a hybridization of the LES and RANS approaches for the modeling of 3D unsteady convection during CZ silicon crystal growth. The model provides a proper prediction of turbulent viscosity in the melt core and in the vicinity of solid surfaces. An industrial CZ melt configuration has been considered with the model and the calculations have been compared to available experimental data for different crucible rotations. The comparison has shown that the model is predictive with respect to the average temperature difference in the melt and the spectral characteristics of the thermal fluctuations.

ACKNOWLEDGEMENTS

We would like to thank I.Yu. Evstratov, E.V. Yakovlev, and N.G. Ivanov for fruitful discussions and for help with numerical realization. The authors acknowledge Wacker Siltronic for support of the work.

REFERENCES

Assaker, A., Van der Bogaert, N., and Dupret, F., 1997, "Time-dependent simulation of the growth of large silicon crystals by Czochralski technique using a turbulent model for melt convection", J. Cryst. Growth, vol. 180, pp. 450-460.

Basu, B., Engen, S., Breuer, M., and Durst, F., 2000, "Three-dimensional simulation of flow and thermal field in a Czochralski melt using a block-structed finite-volume method", J. Cryst. Growth, vol. 219, pp. 123-143.

Chien, K. Y., 1982, "Predictions of channel and boundary-layer flows with low-Reynolds-number turbulence model, AIAA Journal, vol. 20, pp. 33- 38.

Dornberger, E., Tomzig, E., Seidl, A., Schmitt, S., Leister, H.-J., Schmitt, Ch., and Müller, G., 1997, "Thermal simulation of the Chochralski silicon growth process by three different models and comparison with experimental results", J. Cryst. Growth, vol. 180, pp. 461-467.

Egorov, Yu.E., Makarov, Yu.N., Rudinsky, E.A., Smirnov, E.M., and Zhmakin, A.I., 1998, "Modelling analysis of oxygen transport during Czochralski growth of silicon crystals", Mat. Res. Soc. Symp. Proc., vol. 490, pp. 181-186.

Gräbner, O., Mühe, A., Müller, G., Tomzig, E., Virbulis, J., and von Ammon, W., 2000, "Analysis of turbulent flow in silicon melts by optical temperature measurement", Mat. Science and Eng. B, vol. 73, pp. 130-133.

Kalaev, V.V., Evstratov, I.Yu., Makarov, Yu.N., Smirnov, E.M., and Zhmakin, A.I., 2000, "Numerical modeling of Czochralski silicon crystal growth", ECCOMAS CD-ROM Proceeding

Kishida, Yu., and Okazawa, K., 2000, "Geostrophic turbulence in CZ silicon crucible", J. Cryst. Growth, vol. 198/199, pp. 135-140.

Lipchin, A., and Brown, R.A., 1999, "Comparison of three turbulence models for simulation of melt convection in Czochralski crystal growth of silicon", J. Cryst. Growth, vol. 205, pp. 71-91.

Lipchin, A., and Brown, R.A., 2000, "Hybrid finite-volume/finite-element simulation of heat transfer and melt turbulence in Czochralski crystal growth of silicon", J. Cryst. Growth, vol. 216, pp. 192-203.

Mühe, A., Backofen, R., Fainberg, J., Müller, G., Dornberger, E., Tomzig, E., and von Ammon, W., 1999, "Oxygen distribution in silicon melt during a standard Czochralski process studied by sensor measurements and comparison to numerical simulation", J. Cryst. Growth, vol. 198/199, pp. 409-413.

Müller, G., Mühe, A., Backofen, R., Tomzig, E., and von Ammon, W., 1999, "Study of oxygen transport in Czochralski growth of silicon", Microelectronic Engineering, vol. 1, pp.135-147.

Seidl, A., Müller, G., Dornberger, E., Tomzig, E., Rexer, B., and von Ammon, W., 1998, "Turbulent melt convection and its implication on large diameter silicon Czochralski crystal growth", J. Electrochem. Soc., vol. 136, pp. 417-428.